Digital tomosynthesis mammography using a parallel maximum likelihood reconstruction method

Tao Wu*[a], Juemin Zhang[b], Richard Moore[a], Elizabeth Rafferty[a], Daniel Kopans[a], Waleed Meleis[b], David Kaeli[b],
[a]Radiology Department, Massachusetts General Hospital, Boston, MA 02114
[b]Dept. of Electrical and Computer Engineering, Northeastern University, Boston, MA 02115

ABSTRACT

A parallel reconstruction method, based on an iterative maximum likelihood (ML) algorithm, is developed to provide fast reconstruction for digital tomosynthesis mammography. Tomosynthesis mammography acquires 11 low-dose projections of a breast by moving an x-ray tube over a 50º angular range. In parallel reconstruction, each projection is divided into multiple segments along the chest-to-nipple direction. Using the 11 projections, segments located at the same distance from the chest wall are combined to compute a partial reconstruction of the total breast volume. The shape of the partial reconstruction forms a thin slab, angled toward the x-ray source at a projection angle 0º. The initial partial reconstruction is computed on a single processing node. The reconstruction of the total breast volume is obtained by merging the partial reconstructions. The overlap region between neighboring partial reconstructions and neighboring projection segments is utilized to compensate for the incomplete data at the boundary locations present in the partial reconstructions. A serial execution of the computation is compared to a parallel implementation, using clinical data. The serial code was run on a PC with a single PentiumIV 2.2GHz CPU. The parallel implementation was developed using MPI and run on a 64-node Linux cluster using 800MHz Itanium CPUs. The serial reconstruction for a medium-sized breast (5cm thickness, 11cm chest-to-nipple distance) takes 115 minutes, while a parallel implementation takes only 3.5 minutes (on 64 processing nodes). The reconstruction time for a larger breast using a serial implementation takes 187 minutes, while a parallel implementation takes 6.5 minutes. No significant differences were observed between the reconstructions produced by the serial and parallel implementations.

Keywords: tomosynthesis, breast imaging, 3-D reconstruction, parallel computation, iterative reconstruction

1. INTRODUCTION

Tomosynthesis is an imaging technique that provides planar information of an object from a set of discrete x-ray projections[1]. In this technique, image slices at arbitrary locations within the object are retrospectively reconstructed from a single scan. Tomosynthesis mammography has been investigated to solve the breast tissue superimposition problem[2-5]. Conventional two-dimensional (2-D) mammography is currently the most effective screening tool for the early detection of breast cancer. However, there are about 30% of breast cancers missed by mammography, primarily due to overlapped normal breast tissue that obscures the cancer[6]. Meanwhile, the superimposed normal tissues sometimes look like a tumor with ill-defined margins on a mammogram, which generates a large number of unnecessary callbacks. At the Massachusetts General Hospital (MGH), false-positive callback rate caused by superimposed normal breast tissues is approximately 25%. As a three-dimensional (3-D) technique, tomosynthesis mammography provides more accurate diagnosis by separating overlapping breast tissues.

A prototype breast tomosynthesis system has been co-developed by MGH and General Electric Global Research[2] (**Fig. 1**). A flat panel detector is used to acquire 11 projections of the breast over a 50˚ angular range (recorded at ~5º angular steps). The breast and the detector are stationary during the acquisition. The breast volume is reconstructed from the projections. A tomosynthesis reconstruction consists of multiple 1 mm thick slices parallel to the detector plane.

Each tomosynthesis projection is acquired with very low x-ray exposure. The total dose from 11 projections is about 50% higher than that generated during a single screen-film mammogram. Conventional screening mammography takes a medio-lateral oblique (MLO) view and a cranio-caudal (CC) view for a breast. Tomosynthesis only requires the MLO

view because 3-D structural information is available and because a MLO view provides the most complete coverage of the whole breast. Therefore, the patient is exposed to a lower dose with tomosynthesis than with conventional two-view mammography. In tomosynthesis, the breast is compressed in the same way as in conventional mammography. The total image acquisition time for 11 projections is about 7 seconds. Patient motion is reduced by breast compression and rapid image acquisition.

The development of tomosynthesis reconstruction algorithms is challenging because only a limited number of low-dose projections, acquired over a limited angular range, are available. Different types of tomosynthesis reconstruction methods have been explored. The conventional algorithm is called *shift-and-add*[2]. Using this algorithm, projection images taken at different angles are shifted and added together to generate an in-focus image slice, located at a defined depth under the breast surface. The amount of the shift is adjusted so that the visibility of features in this slice is enhanced, while the information of out-of-focus features is blurred. Filtered back-projection based algorithms have also been investigated, in which dedicated filters are designed based on the tomosynthesis geometry and the features of interest[7-9]. Matrix inversion algorithm have also been developed to attempt to balance the quality of the high-frequency signal and the low-frequency signal during reconstruction[10,11]. Iterative reconstruction algorithms represent another class of reconstruction methods, in which a model of the breast volume is iteratively updated until the current output satisfies a predefined objective function[5,12]. The objective function determines the quality the reconstructed solution. Dobbins and Godfrey have surveyed tomosynthesis methods extensively, as well as the clinical applications[13].

For tomosynthesis mammography, we have elected to use an iterative maximum likelihood (ML) algorithm for our clinical studies[5]. The objective function in the ML algorithm is the likelihood function $L = P(Y|u)$, which computes the probability of generating the projections Y obtained in the experiment, given a 3-D model of the attenuation coefficients u. Clinical studies have shown that cancers missed in 2-D mammograms due to superimposed tissues can now be found in tomosynthesis reconstructions. The number of false-positive callbacks caused by superimposed normal tissues is also reduced using tomosynthesis**. Our iterative ML algorithm has been shown to produce tomosynthesis reconstructions of excellent quality. However, this algorithm requires intensive computation. It takes 1-3 hours to get an 8-iteration reconstruction of a breast volume. The computation time must be significantly reduced for clinical applications.

2. METHODOLOGY

A parallel reconstruction algorithm has been developed to perform tomosynthesis reconstruction on a 64-node based computing platform. This method uses the same ML algorithm used in the serial implementation. In the parallel method, the reconstruction of a big breast volume is divided into multiple partial reconstructions. Each partial reconstruction is executed on a CPU node of the cluster. When all partial reconstructions are computed, reconstruction of the whole breast volume is generated from these partial reconstructions. In our implementation, the number of partial reconstructions is equal to the number of cluster nodes (one partial reconstruction per node). Therefore the total time includes the time one partial reconstruction consumes, plus the time to compute the projection partition, to perform volume retrieval, and to transfer data.

2.1. Data partition

For efficient parallel computation, one would want to limit the amount of inter-node communication. In this work, data partitioning is used such that a computation on one cluster node is independent of the computation performed on any other node. A tomosynthesis projection is divided into multiple segments along the chest-to-nipple direction (**Fig. 2A**). In projection i, the *j-th* segment from the chest wall side is denoted as S_{ij}. From the 11 projection images, segments with the same index j are grouped and used for a partial reconstruction of the breast volume.

The partition of the reconstructed volume is determined by the way in which the projection images are partitioned. In our approach, the reconstruction volume is partitioned along the chest-to-nipple direction, just as the projection segments (**Fig. 2B**). The shape of a partial breast volume is a thin slab angled toward the x-ray source at a 0° projection angle. The extension of the mid-plane of the partial reconstruction passes through the 0° x-ray source. The size of a partial reconstruction is the area of the corresponding projection segment multiplied by the breast thickness. Since the x-ray is contained in the extension of the mid-plane, the shape of a partial reconstruction is slightly different than its

neighbors. The angle made by the intersection of the mid-plane of a partial reconstruction and the detector plane increases as the partial reconstruction gets closer to the chest wall side. Under cone-beam geometry, data partitioning insures that most projection data required for a partial reconstruction is contained in the corresponding projection segments.

2.2. Overlap between partitioned data

Because of the cone-beam geometry, some projection data required for a partially reconstructed volume is missing using of the partition scheme described above. The missing projection data results in incomplete data at the boundaries of the partial reconstructions (**Fig. 3**, the actual shape of the incomplete-data region is not shown). Since the incomplete-data region only occurs at the boundary, the size of the projection segments and the size of partial volumes is increased so that the geometrical of a bad-data region in a partial reconstruction is overlapped with a correct data region in the neighboring partial reconstruction. With sufficient overlap, we can guarantee that, for any location within the breast volume, valid reconstruction data can always be retrieved from the partial reconstructions. Therefore, the incomplete data regions are compensated by allowing for overlap (data redundancy) between neighboring projection segments and between neighboring partial reconstructions (**Fig. 2** and **3**).

2.3. Volume merging

Reconstruction of a complete breast volume is obtained by merging partial reconstructions. To allocate the value of a voxel in the breast volume, the location of this voxel is first calculated. A partial volume that covers this location is then identified and the value for the voxel at this location is recovered from the selected partial reconstruction. If the voxel is located in the overlap region between two partial reconstructions, the value will be retrieved from the partition with a mid-plane that is closer to this voxel. The reasoning behind this choice is based on the fact that the good-data region in a partial reconstruction is close to the mid-plane, while the incomplete-data region is located at the boundary. For example, if the voxel being generated is located in incomplete-data region 1 of the partially reconstructed volume *j* in **Fig. 3**, the volume-merging scheme will find two partial reconstructions *j* and *j-1*, both of which cover the location of this voxel. The scheme will choose the partial reconstruction *j-1* to retrieve the voxel value because the location of this voxel is much closer to the mid-plane of partial reconstruction *j-1*, which is in the good-data region. Our volume-merging scheme makes sure that the reconstruction of the whole breast volume can always be retrieved from good-data regions in the partial reconstructions.

3. DATA

We have selected two different clinical cases to compare the performance of the serial and the parallel ML implementations. The first case is a medium-sized breast, with a thickness of 5 cm, and with a chest-to-nipple distance of 11 cm (1100×2304×50 voxels in reconstruction). The second case is a very large breast, with a thickness of 7 cm and a chest-to-nipple distance of 14 cm (1400×2304×70 voxels in reconstruction). These cases provide us with two reference points. We can measure the time needed to process a typical and a computationally-intensive tomosynthesis reconstruction. The serial implementation, which reconstructs the complete breast volume as a single segment, was executed on a single-CPU workstation. This system possesses a 2.2 GHz PentiumIV CPU. Our parallel implementation, which uses a multi-segment scheme, was executed on a 64-node Itanium-based system (a 800MHz 64-bit architecture), interconnected by a 1Gb Myrinet network switch. A 50% overlap between neighboring projection segments was used, which provided very satisfactory results for these two cases. The optimal size of the overlap between neighboring projection segments remains an open problem to be studied in future work.

4. RESULTS

For the medium-sized breast dataset, an 8-iteration reconstruction took 115 minutes using the serial implementation run on the PC workstation. The parallel reconstruction implemented on the 64-node cluster took around 3.5 minutes. Reconstructing the larger breast dataset took 187 minutes using the serial code and 6.5 minutes using the parallellized code. Computation time was significantly reduced in our parallellized implementation.

We next compare the quality of the serial and parallel reconstructions. Three reconstruction slices, located at 5 mm, 18 mm and 33 mm under the skin, were compared from the reconstruction. Results from the single-segment serial implementation (**S**) and the multi-segment parallellized implementation (**M**), as well as an image generated capturing the difference between the two methods (**S-M**), are shown in **Fig. 4**. As we can see, no significant difference is evident between the reconstructed images produced by two implementations. Only a small geometric mismatch (2-3 pixels) was found to exist between the two results. The mismatch was caused by rounding operations performed during data partitioning and volume merging. The pixel value in the difference image was about 2-3% of the pixel value in the reconstructed slice. From the reconstructions of the larger breast, three reconstructed slices located at depths of 10, 30 and 50 mm under the skin were selected for comparison (**Fig. 5**). The pixel values in the difference image only changed in 1-2% of the pixel values in the reconstruction slice. The reconstruction using the parallel implementation provides equivalent diagnostic information as produced by the original serial code.

5. CONCLUSIONS

A multi-segment parallel reconstruction algorithm has been developed, which provides fast tomosynthesis reconstruction on a 64-node cluster. The fidelity of this implementation tested using both a medium sized breast dataset, as well as a much larger dataset. No significant differences in image quality were observed between the parallel implementation and the original serial method. In our future work, we plan to experiment with tradeoffs between the size of the overlap region and the resulting image quality.

ACKNOWLEDGEMENTS

This work is supported by research funding from the Breast Imaging Division of Radiology Department, Massachusetts General Hospital, by the Institute for Complex Scientific Software (ICSS) at Northeastern University, the Center for Subsurface Sensing and Imaging Systems (CenSSIS) under the Engineering Research Centers Program of the NSF (Award Number EEC-9986821), and by an NSF Major Research Instrumentation Grant (Award Number MRI-9871022).

REFERENCES

1. D. G. Grant, “Tomosynthesis: A three-dimensional radiographic imaging technique,” IEEE Trans. Biomed. Eng. **19**, 20-28, (1972).
2. L. T. Niklason, B. T. Christian, L. E. Niklason, D. B. Kopans, D. E. Castleberry, B. H. Opsahl-Ong, C. E. Landberg, P. J. Slanetz, A. A. Giardino, R. M. Moore, D. Albagi, M. C. DeJule, P. A. Fitzgerald, D. F. Fobare, B. W. Giambattista, R. F. Kwasnick, J. Liu, S. J. Lubowski, G. E. Possin, J. F. Richotte, C-Y Wei and R. F. Wirth, "Digital tomosynthesis in breast imaging,” Radiology, **205**, 399-406 (1997).
3. S. Suryanarayanan, A. Karellas, S. Vedantham, S. J. Glick, C. J. D’Orsi, S. P. Baker, and R. L. Webber, “Comparison of tomosynthesis methods used with digital mammography,” Acad. Radiol. **7**, 1085-1097 (2000).
4. S. Suryanarayanan, A. Karellas, S. Vedantham, S. P. Baker, S. J. Glick, C. J. D’Orsi, and R. L. Webber, “Evaluation of linear and nonlinear tomosynthetic reconstruction methods in digital mammography,” Acad. Radiol. **8**, 219-224 (2001).
5. T. Wu, A. Stewart, M. Stanton, T. McCauley, W. Phillips, D. B. Kopans, R. H. Moore, J. W. Eberhard, B. Opsahl-Ong, L. Niklason, and M. B. Williams, "Tomographic mammography using a limited number of low-dose cone-beam projection images," Med. Phys. **30** (3), 365-380 (2003).
6. D. B. Kopans, *Breast Imaging*, 2nd ed. (Lippincott Williams & Wilkins, 1997).
7. H. Matsuo, A. Iwata, I. Horiba, and N. Suzumura, “Three-dimensional image reconstruction by digital tomosynthesis using inverse filtering,” IEEE Trans. Med. Imaging, **12** (2), 307-313 (1993).
8. G. Lauritsch and W. Haerer, “A theoretical framework for filtered backprojection in tomosynthesis,” Proc SPIE Medical Imaging, **3338**, 1127-1137 (1998).
9. G. M. Stevens, R. Fahrig, and N. J. Pelc, “Filtered backprojection for modifying the impulse response of circular tomosynthesis,” Med. Phys. **28** (3), 372-380 (2001).
10. R. J. Warp, D. G. Godfrey, J. T. Dobbins III, “Applications of matrix inverse tomosynthesis,” Proc. SPIE Medical Imaging, **3977**, 376-383 (2000).

11. D. J. Godfrey, R. J. Warp, and J. T. Dobbins, "Optimization of matrix inversion tomosynthesis," Proc. SPIE Medical Imaging, **4320**, 696-704 (2001).
12. P. Bleuet, R. Guillemaud, I. Magnin, and L. Desbat, "An adapted fan volume sampling scheme for 3D algebraic reconstruction in linear tomosynthesis," IEEE Trans. Nucl. Sci. **49** (5), 2366-2372 (2002).
13. J. T. Dobbins III and D. J. Godfrey, "Digital x-ray tomosynthesis: current state of the art and clinical potential," Phys. Med. Biol. **48** (19), R65-R106 (2003).

*Email: twu2@partners.org; phone: 617-726-3694; fax: 617-726-1074

** The clinical studies on tomosynthesis were presented in RSNA 2002 and ARRS 2003:

1) E..A. Rafferty, D. Georgian-Smith, D. B. Kopans, D. A. Hall, R. H. Moore, T. Wu T, K. A. McCarthy, L. Niklason, E. Yeh, M. M. Staffa, "Comparison of full-field digital tomosynthesis with two view conventional film screen mammography in the prediction of lesion malignancy," RSNA annual meeting, 2002.

2) E. A. Rafferty, D. Georgian-Smith, D. B. Kopans, R. H. Moore, T. Wu, L. Niklason, D. A. Hall, K. A. McCarthy, E. Yeh, M. M. Staffa, "Comparison of full-field digital tomosynthesis and conventional two view film screen mammography in lesion detection and assessment of lesion conspicuity," ARRS annual meeting, 2003

3) E. A. Rafferty, D. Georgian-Smith, D. B. Kopans, R. H. Moore, T. Wu, L. Niklason, D. A. Hall, K. A. McCarthy, E. Yeh, M. M. Staffa, "Evaluation of the call-back rate for screening mammography using full-field digital tomosynthesis versus conventional film-screen mammography," ARRS annual meeting, 2003.

CAPTIONS

Fig. 1 Breast tomosynthesis system, (A) Front view of the system; (B) Side view of the system. Eleven projections are acquired over a 50º angular range (~5º angular steps). During the acquisition, the breast and the detector are stationary and the x-ray tube is rotated. An a-Si flat panel detector (100μm pixel size) is used to record images. No anti-scatter grid is used. An amorphous Si (CsI:Tl) flat-panel detector (1800×2304 pixels, 0.1 mm pixel size) is used to record projection images. A Rh/Rh target/filter combination is used to image 3-8 cm thick breasts. The exposure time for each projection is 0.1~0.2 second and detector readout time is about 0.3 second. The x-ray tube is moved to the next position during the detector readout. The total image acquisition time for 11 projections is about 7 seconds.

Fig. 2 Partition of the projection and the reconstruction volume. (A) A projection image is divided into multiple segments along the chest-to-nipple direction. Segments with the same index *j* from 11 projections are grouped and used to reconstruct a partial breast volume *j*. (B) The reconstruction of the breast volume is also partitioned along the chest-to-nipple direction. The shape of a partial reconstruction volume is a slab tilted toward the x-ray source at 0° projection angle. The x-ray source at 0° is located in the extension of the mid-plane of the partial reconstruction volume. The shape of a partial reconstruction volume is different than another one (such as partial volumes *j* and *j-1*). The size of a partial reconstruction volume *j* is the area of the projection segment *j* multiplied by the breast thickness. In (A) and (B), overlap between neighbor projection segments and between neighbor partial reconstruction volumes is illustrated.

Fig. 3 Reconstructions of two overlapped neighbor partial reconstruction volumes *j* and *j-1*. Bad-data regions exist in boundaries of the reconstructions (the shape of the bad-data region is not as illustrated). In this illustration, the overlap is large enough so that each bad-data region in a partial reconstruction volume is overlapped with a good-data region of the neighbor partial reconstruction volume (bad-data region 1 of volume *j-1* is compensated by volume *j-2*; bad-data region 2 of volume *j* is compensated by volume *j+1*). In volume merging step, the reconstruction of the whole breast is retrieved using only the good-data regions of the partial reconstruction volumes. For a voxel located in the overlap region, its value is retrieved from the partial reconstruction volume whose mid-plane is closer to this voxel because the good-data region of a partial volume is close to the mid-plane while the bad-data region is located at the boundary.

Fig. 4 Reconstructions of a regular-sized breast (5 cm thickness, 11 cm chest-to-nipple distance) using the non-parallel and parallel algorithms are compared. Reconstruction slices using the single segment non-parallel algorithm (**S**), the multi-segment parallel algorithm (**M**); and the difference between these two algorithms (**S-M**) are shown in three columns. Slices located at 5 mm (sub-skin), 18 mm (a benign tumor in the middle, close to the chest wall), and 33 mm (normal breast tissues) under the skin were compared. The difference in pixel value between the two reconstructions is about 2-3%. A small geometric mismatch was observed in this case too. No significant difference between the results from the two algorithms was found.

Fig. 5 Reconstructions using the non-parallel and parallel algorithms are compared. This case is a very large breast (7 cm thickness, 14 cm chest-to-nipple distance). The first column (**S**) shows the reconstruction slices using the single segment non-parallel ML algorithm; the second column (**M**) shows the slices using the multi-segment parallel algorithm; the difference between these two algorithms is shown in the third column (**S-M**). Slices located at 0 mm (breast surface where blood vessels are visible), 20 mm (breast tissue, a mass with smooth boundary at the bottom, and a lymph node on the top left), and 40 mm (a cancer in the middle) under the skin were selected from the reconstruction. The difference in pixel value between the two reconstructions is about 1-2%. A small geometric mismatch (2-3 pixels) exists, which may be caused by the rounding-off error in the implementation of data partition and partial volume merging.

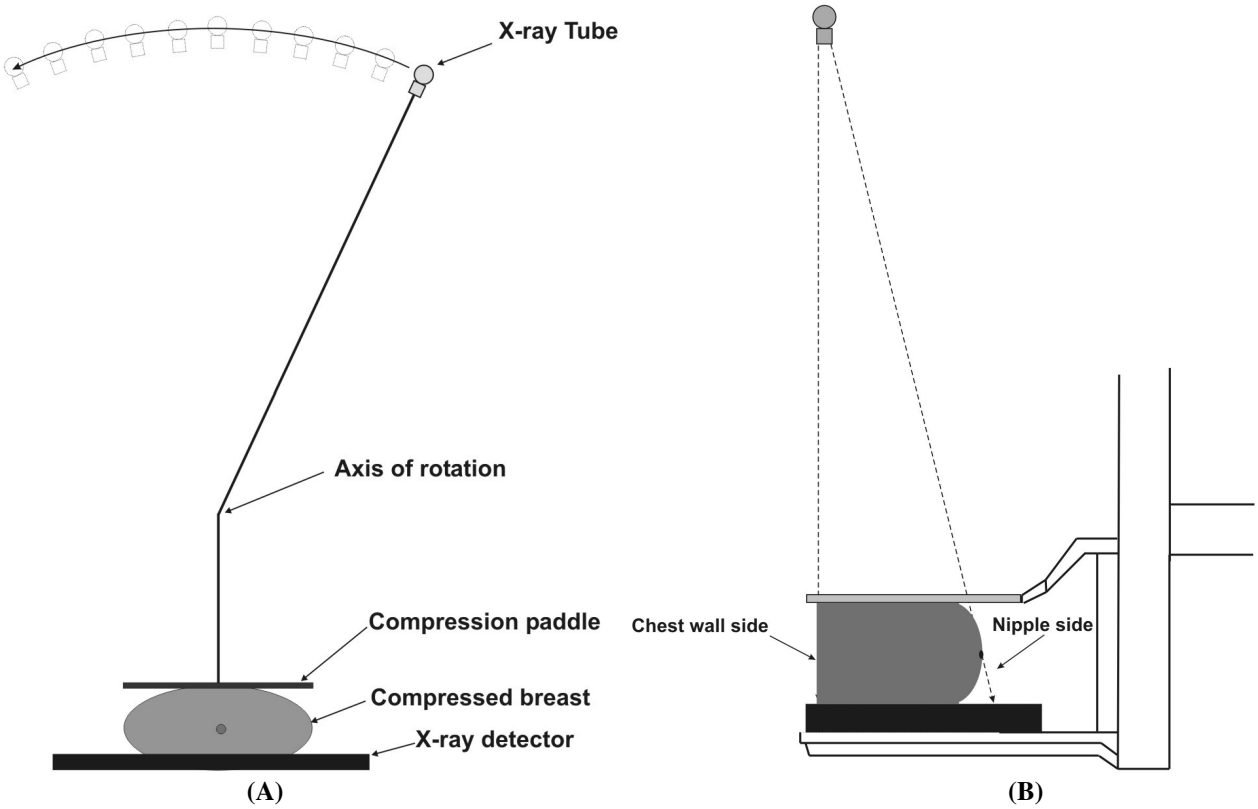
X-ray Tube
Axis of rotation
Compression paddle
Compressed breast
X-ray detector
(A)
Chest wall side
Nipple side
(B)

Figure 1

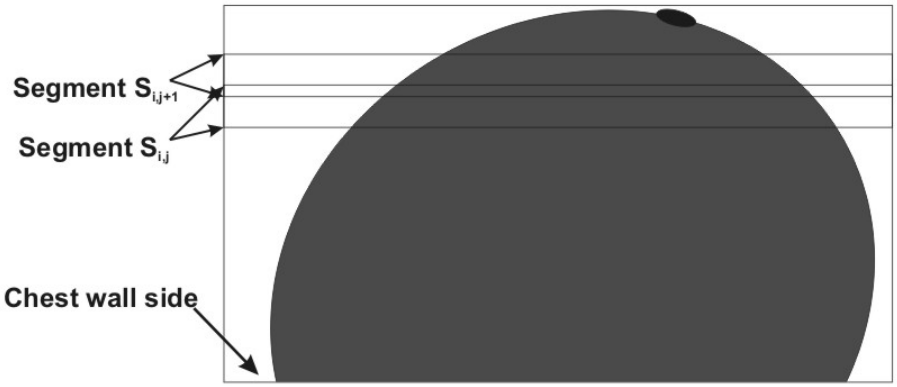

Figure 2 (A)

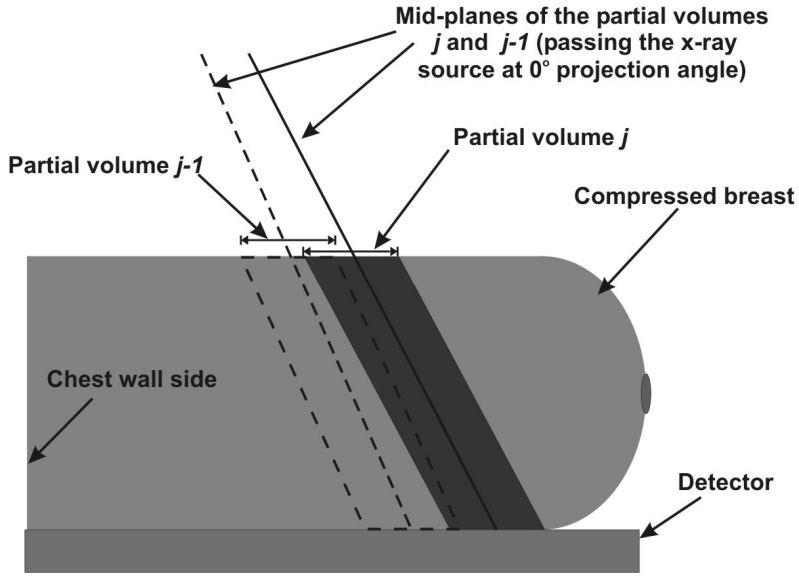

Figure 2 (B)

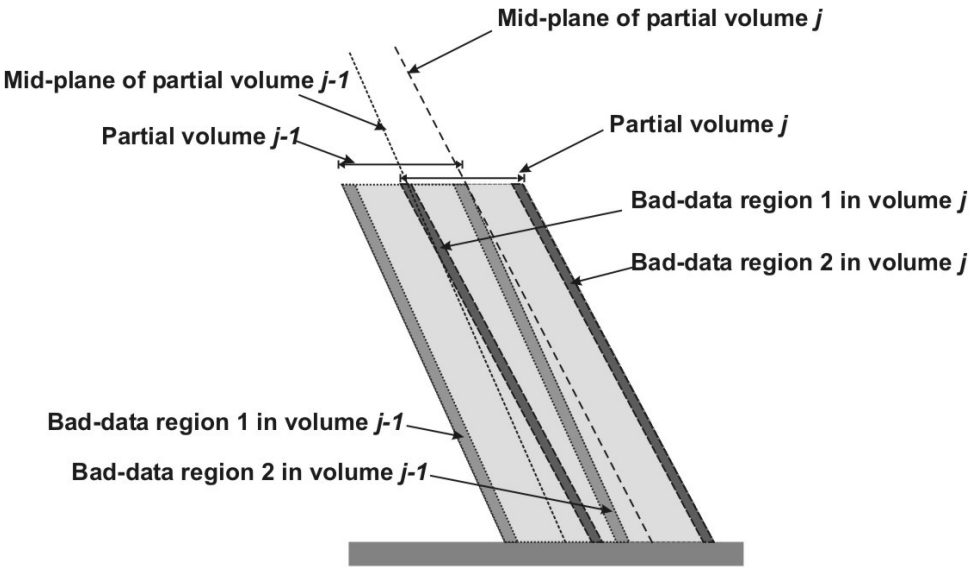
Mid-plane of partial volume *j*
Mid-plane of partial volume *j-1*
Partial volume *j-1*
Partial volume *j*
Bad-data region 1 in volume *j*
Bad-data region 2 in volume *j*
Bad-data region 1 in volume *j-1*
Bad-data region 2 in volume *j-1*

Figure 3

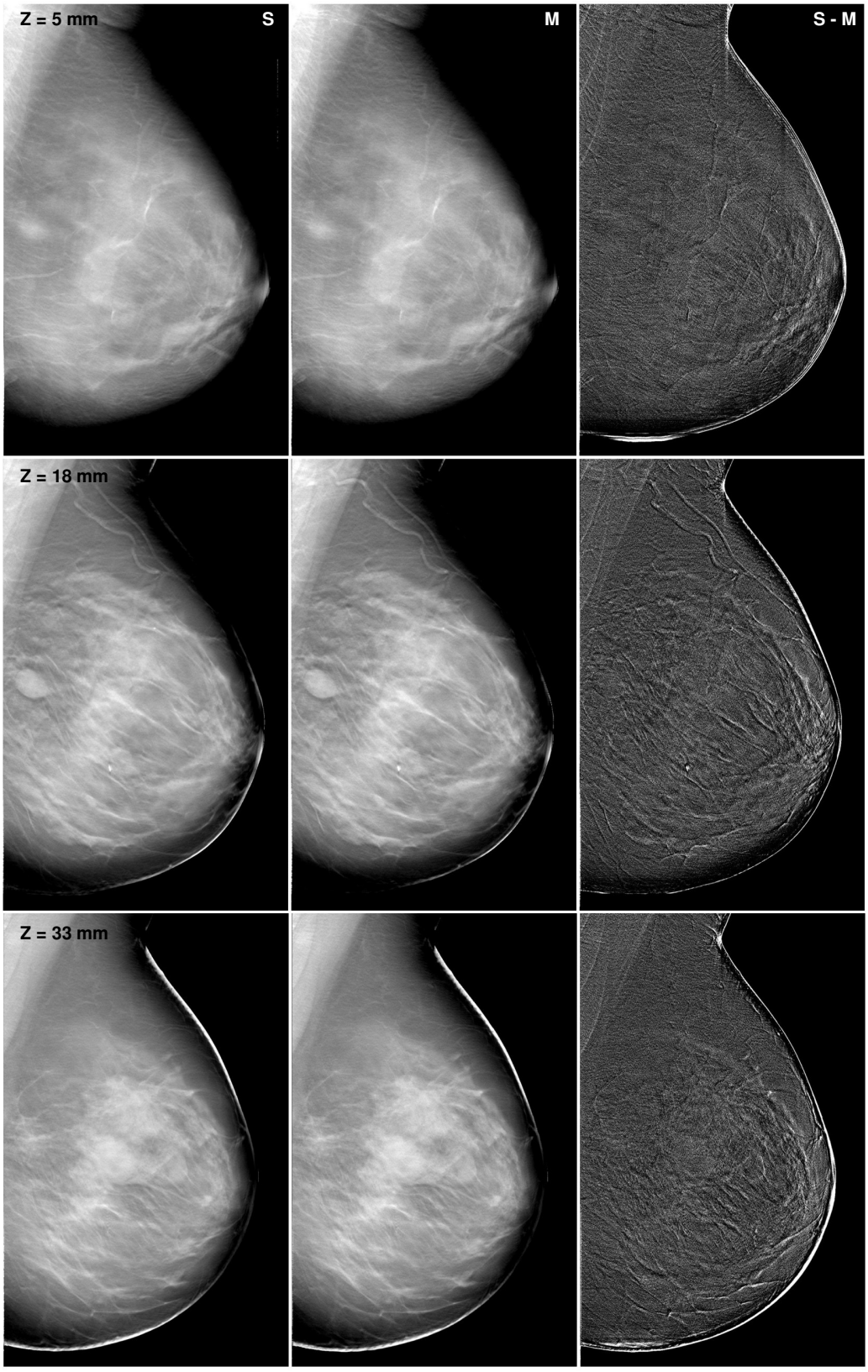

Figure 4

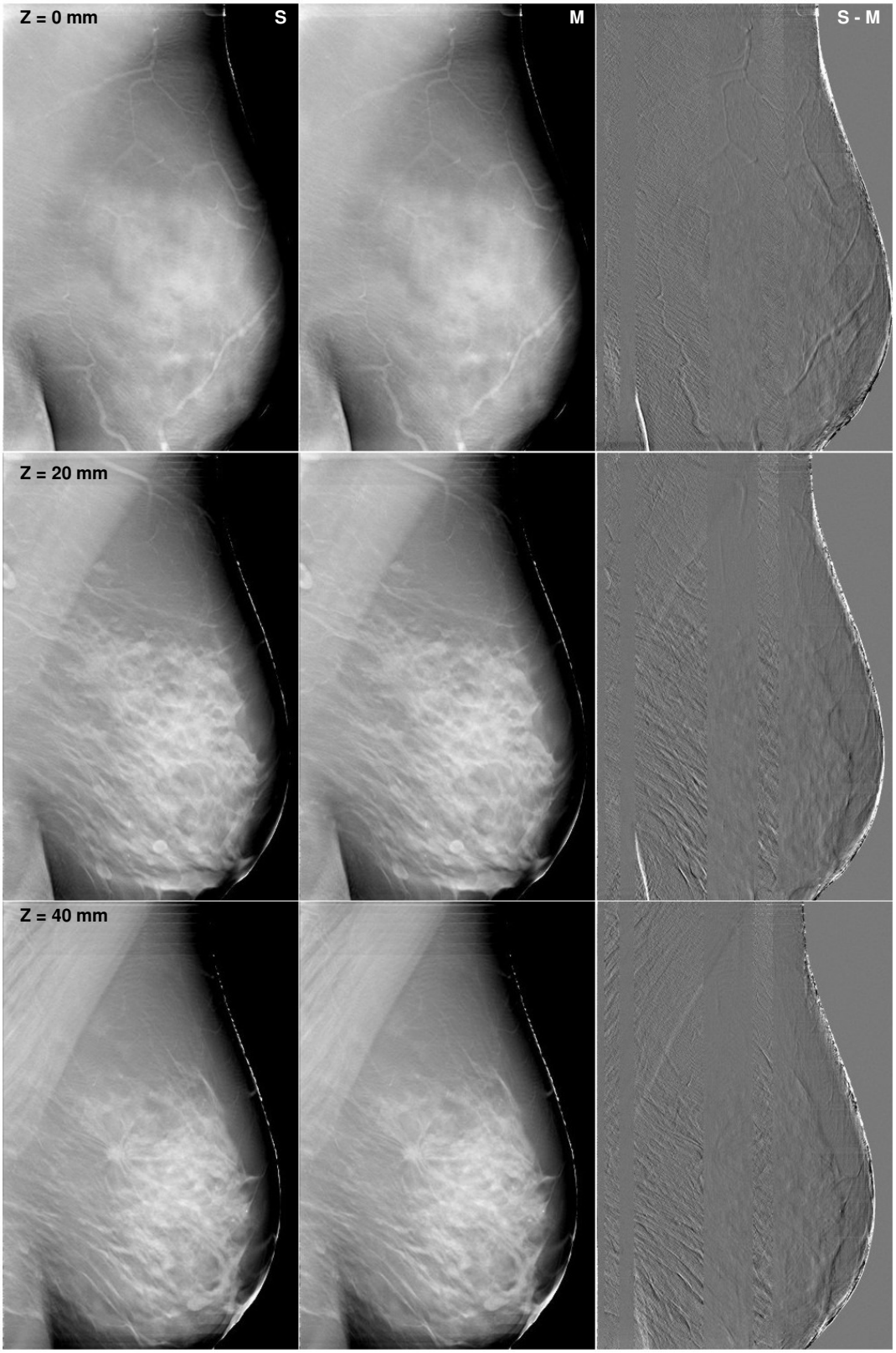

Figure 5